

Calibration and data fusion solution for the miniature attitude and heading reference system

David Jurman*, Marko Jankovec, Roman Kamnik, Marko Topič

Faculty of Electrical Engineering, University of Ljubljana, Tržaška cesta 25, SI-1000, Ljubljana, Slovenia

Received 29 November 2006; received in revised form 10 April 2007; accepted 8 May 2007

Available online 17 May 2007

Abstract

Development, calibration and alignment of a miniature magnetic and inertial measurement unit, which is used as an attitude and heading reference system, are presented. Several guidelines were followed during the design process to make the magnetic and inertial measurement unit suitable for various kinds of applications, thus the system is designed both as small as possible but still modular, consisting of three inertial sensor units, a magnetic sensor unit and a control unit.

Complete calibration and alignment procedure is described and an adaptive Kalman filter concept for fusing various sensors' attitude and heading data is introduced and discussed. The characteristics of the magnetic and inertial measurement unit as an attitude and heading reference system are evaluated. The algorithm showed remarkable performance in the orientation determination as the average root mean square error was less than 1.2° over the entire applicable operating range.

© 2007 Elsevier B.V. All rights reserved.

Keywords: Inertial measurement unit; Electronic compass; Sensor calibration; Data fusion; Kalman filter

1. Introduction

The progress in micro electro-mechanical system (MEMS) and anisotropic-magneto-resistive (AMR) technology has enabled engagement of inertial MEMS and magnetic AMR sensors in broad spectrum of consumer market applications. Nowadays, a small-size inertial measurement unit (IMU) and electronic compass with off-the-shelf sensors are found in variety of applications, such as unmanned aerial [1] and underwater vehicles [2], handheld navigation devices, human motion tracking [3] and many more.

Despite highly automated production process, the parameters of the contemporary low-cost MEMS and AMR sensors may deviate from a piece to a piece. In our case, the vendor's data of the chosen sensors' sensitivity deviations are $\pm 10\%$ for the MEMS rate gyroscope [4] or even $\pm 25\%$ for the AMR magnetic sensor [5]. Therefore great concern must be paid to the calibration and alignment of the sensors on one side and on the other side advanced sensor data fusion concepts must be applied to achieve desired performance.

The scope of this paper is to present methods, how to build, calibrate, align and maximize the performance of such a low-cost sensor system. For this reason, a miniature magnetic and inertial measurement unit (MIMU) has been developed. The unit was calibrated and aligned according to methods from [6,7] and [8] but modified and adapted to suit the unified accelerometer, gyroscope and magnetometer sensor model. To compute the attitude and heading an effective adaptive Kalman filter data fusion technique was developed and implemented. The whole system was tested as an attitude and heading reference system (AHRS) and the performance was evaluated using an optical kinematic measurement system.

2. Theoretical background

2.1. Orientation representation

Attitude and heading (the orientation) of a rigid body expressed in the inertial coordinate frame can be represented in different ways such as direction cosine matrix (DCM), Euler angles or quaternions.

The DCM is the straightforward method to present the orientation, but the weakness of this approach is that nine parameters

* Corresponding author. Tel.: +386 14768321.

E-mail address: david.jurman@fe.uni-lj.si (D. Jurman).

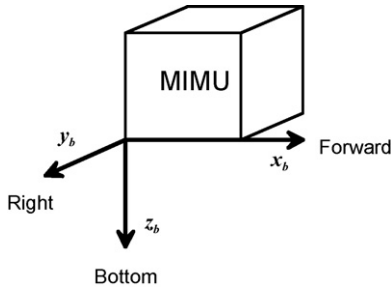


Fig. 1. Body frame fixed to the MIMU's casing.

are needed. If the quaternions are used, only four parameters are required, however, the quaternion representation of the orientation needs to be transformed before it can be displayed in easily understood format. For the orientation representation in our case the aerospace sequence Euler angles (ψ -heading, ϑ -elevation, ϕ -bank) are used [9]. This parameterization is chosen because of its intuitive nature, despite the singularities and nonlinearity of kinematic equations. Additional motive was the simple data fusion algorithm design, since the orientation information provided by the accelerometers and the electronic compass is represented in this way.

The body coordinate frame is fixed to the MIMU's casing, the x_b -axis points in the forward direction and it is aligned with the roll axis, the z_b -axis (yaw axis) points to the bottom of the MIMU and the y_b -axis (pitch) rounds up the right-handed orthogonal coordinate system (Fig. 1). The inertial coordinate frame is so called North, East, Down (NED) frame. The axes x_i and y_i lie on the local level tangent plane. The x_i -axis points to the north and the y_i -axis to the east. The z_i -axis completes the frame by pointing to the Earth's centre (Fig. 2).

By means of the MIMU the attitude and heading can be determined by either of two complementary approaches. A triad of rate gyros or a combination of a tri-axis accelerometer and an electronic compass can be used. Since each approach has its advantages and disadvantages, the combination of both approaches leads to the highest fidelity and accuracy of the orientation estimation.

2.2. Rate gyro approach

Rate gyro is used to compute the orientation by the integration of the rigid body kinematic equations. Roll, pitch and yaw angular rates (ω_x , ω_y , ω_z) measured by gyros in MIMU's body frame

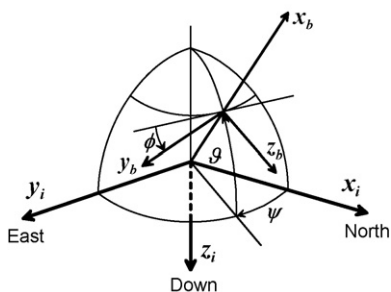


Fig. 2. Orientation of the body frame expressed in the inertial frame.

are transformed into the reference frame Euler angle rates: $\dot{\psi}$, $\dot{\vartheta}$ and $\dot{\phi}$ (Eq. (1)). The Euler angle rates are afterwards numerically integrated and orientation is obtained. Due to the drift of the null bias point and the presence of the noise in the gyro output signal, there is a considerable amount of the error accumulating in the gyro-derived orientation. The most important concern is that this accumulating error is unbounded in time, so only the short-term accuracy can be achieved using the rate gyro measurements.

$$\begin{bmatrix} \dot{\psi} \\ \dot{\vartheta} \\ \dot{\phi} \end{bmatrix} = \begin{bmatrix} 0 & \sin \phi \sec \vartheta & \cos \phi \sec \vartheta \\ 0 & \cos \phi & -\sin \phi \\ 1 & \sin \phi \tan \vartheta & \cos \phi \tan \vartheta \end{bmatrix} \begin{bmatrix} \omega_x \\ \omega_y \\ \omega_z \end{bmatrix} \quad (1)$$

2.3. Accelerometer and electronic compass approach

Tri-axis accelerometer or a triad (three orthogonally mounted sensors) of single-axis accelerometers is measuring the resultant of all accelerations acting on the MIMU expressed in the body frame (a_x , a_y , a_z). If the MIMU is not moving and the Coriolis acceleration due to the Earth's rotation is neglected then the gravity is the only acceleration affecting the accelerometer triad. Under these conditions the attitude (elevation- ϑ_{ACC} and bank- ϕ_{ACC}) can be established as stated in Eq. (2) and Eq. (3). Since accelerometer is used as an inclinometer a static activity detection algorithm must be implemented.

$$\vartheta_{ACC} = \arctg \left[\frac{a_x}{\sqrt{a_y^2 + a_z^2}} \right] \quad (2)$$

$$\phi_{ACC} = \arctg \frac{a_y}{a_z} \quad (3)$$

Electronic compass data are used for the heading calculation. In the first place the measurements must be electronically gimballed (Eq. (4)) i.e. the magnetic field vector measured in the body frame (m_x , m_y , m_z) is compensated for the elevation and bank angle to obtain its transform in the inertial frame (m_{xi} , m_{yi} , m_{zi}). Afterwards the heading— ψ_{MAG} is computed using Eq. (5).

$$\begin{bmatrix} m_{xi} \\ m_{yi} \\ m_{zi} \end{bmatrix} = \begin{bmatrix} \cos \vartheta & \sin \phi \sin \vartheta & \cos \phi \sin \vartheta \\ 0 & -\cos \phi & -\sin \phi \\ -\sin \vartheta & \sin \phi \cos \vartheta & \cos \phi \cos \vartheta \end{bmatrix} \begin{bmatrix} m_x \\ m_y \\ m_z \end{bmatrix} \quad (4)$$

$$\psi_{MAG} = \arctg \frac{m_{yi}}{m_{xi}} \quad (5)$$

Heading information provided by the electronic compass is valid only in the homogeneous and undisturbed Earth's magnetic field. If any anomalies in the magnetic field absolute value or in the magnetic field dip angle are noticed then the measurement uncertainty is increased or the current measurement is even invalid.

3. Hardware design process

Since various applications require a specific configuration of sensors, the flexibility of the system design is an important issue. Therefore we have developed a modular system, where more detachable sensor units are connected to a central control unit.

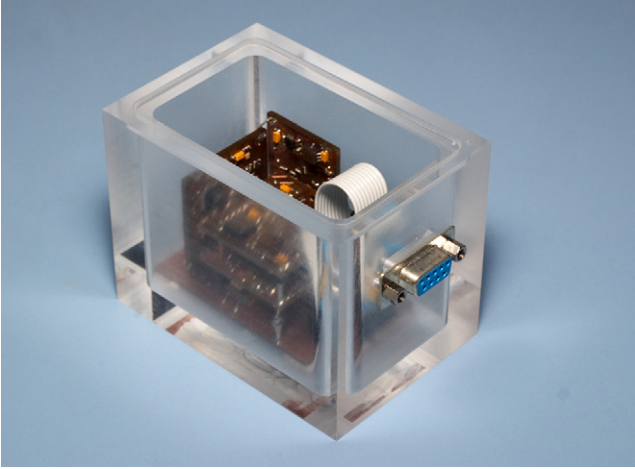


Fig. 3. Realized MIMU in the AHRS configuration.

In the AHRS configuration the MIMU consists of three inertial sensor units (ISU) perpendicular to each other, one magnetic sensor unit (MSU) and a control unit (CU) (Fig. 3) which are enclosed in a cubic plexiglas casing.

Each ISU contains two MEMS sensors: the single-axis angular rate gyroscope (ADXRS150, full-scale range of $\pm 150^\circ/\text{s}$) and two-axis accelerometer (ADXL203, full-scale range of $\pm 1.7 \text{ g}$), both made by the Analog Devices. With such choice of the sensor configuration, translational motion in the plane and rotation about the plane's normal can be detected with a single ISU. With the orthogonal positioning of three ISUs a complete six degree-of-freedom (6 DOF) inertial measurement system was obtained.

MSU comprises two AMR sensors: a single-axis HMC1001 and a dual-axis HMC1002 (produced by the Honeywell) with the full-scale range of ± 2 Gauss, forming a complete three-dimensional electronic compass. MSU also contains a high current flipping circuit for the continuous inverting of the sensors transfer function and a digital to analogue converter for the offset cancellation (the principle similar to the synchronous detection), which reduces the cross-axis effect and temperature drift by more than one order of magnitude [10]. The influence of the MIMU's internal ferromagnetic parts and DC currents are compensated by the means of the calibration procedure, on the other hand the influence of the external magnetic disturbances is minimised by the data fusion algorithm.

During the development process, special attention was paid to the printed circuit board layout and analogue signal processing, not to couple additional noise and interferences to the sensors' output signals.

The data fusion algorithm and the orientation computation can be implemented in the CU, but for the development purposes and testing, it is more convenient that the computation is executed on a personal computer (PC). Therefore, the pre-processed data from the all sensor units are gathered by the ATmega8 microcontroller through the Inter-Integrated Circuit (I²C) bus and passed to the PC (by the RS-232 bus) where all the computation is carried out.

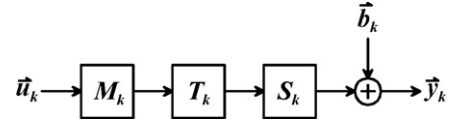


Fig. 4. Model of a sensor triad k .

4. Sensor calibration and alignment

4.1. Sensor model

For the description of sensors, used in the MIMU, a unified mathematical model (Eq. (6)) is used (schematically presented in Fig. 4). Sensors forming the triad have to be mounted perpendicularly to each other and each triad must be aligned to the MIMU's casing. In reality this is difficult to achieve, so an advanced triaxial sensor model is used where all these issues are considered.

Triaxial sensor model is written in the vector form, where index k represents the type of the sensor (g, a or m; gyro, accelerometer or magnetometer, respectively). Measured quantities, outputs and biases of a sensor triad are incorporated in the vectors: \tilde{u}_k , \tilde{y}_k and \tilde{b}_k , respectively; sensitivities are arranged in the matrix S_k . Two other matrices are introduced: the orthogonalization matrix T_k and the alignment matrix M_k . Other effects like compass's cross-axis sensitivity, the gyro acceleration sensitivity and the nonlinearities of the sensors are neglected, since they are suppressed by means of the sensor and hardware design.

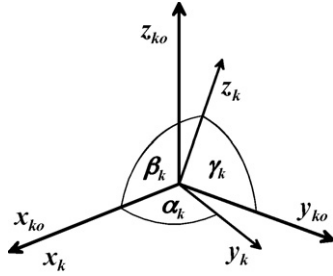
$$\tilde{y}_k = S_k T_k M_k \tilde{u}_k + \tilde{b}_k, \quad k = \text{sensor type}(g, a, m),$$

$$\tilde{u}_k = \begin{bmatrix} u_{kx} \\ u_{ky} \\ u_{kz} \end{bmatrix}, \quad \tilde{y}_k = \begin{bmatrix} y_{kx} \\ y_{ky} \\ y_{kz} \end{bmatrix}, \quad \tilde{b}_k = \begin{bmatrix} b_{kx} \\ b_{ky} \\ b_{kz} \end{bmatrix},$$

$$S_k = \begin{bmatrix} s_{kx} & 0 & 0 \\ 0 & s_{ky} & 0 \\ 0 & 0 & s_{kz} \end{bmatrix}, \quad T_k = \begin{bmatrix} 1 & 0 & 0 \\ \cos \alpha_k & 1 & 0 \\ \cos \beta_k & \cos \gamma_k & 1 \end{bmatrix},$$

$$M_k = \begin{bmatrix} r_{k,11} & r_{k,12} & r_{k,13} \\ r_{k,21} & r_{k,22} & r_{k,23} \\ r_{k,31} & r_{k,32} & r_{k,33} \end{bmatrix} \quad (6)$$

Orthogonalization matrix T_k in Eq. (6) transforms the vector expressed in the orthogonal sensor reference frame ko into the vector expressed in the non-orthogonal sensor reference frame k (Fig. 5). The matrix is constructed using Gram–Schmidt orthogonalization process. The Gram–Schmidt algorithm takes a finite, linearly independent set of vectors and generates an orthogonal set that spans the same subspace. Allowing for that the angles α_k , β_k and γ_k are approximately 90° some approximations may be made without any significant loss of accuracy:

Fig. 5. Orthogonalization of the sensor frame k .

$$T_k = \begin{bmatrix} 1 & 0 & 0 \\ \cos \alpha_k & \sin \alpha_k & 0 \\ \cos \beta_k & \cos \gamma_k & \sqrt{1 - \cos^2 \beta_k - \cos^2 \gamma_k} \end{bmatrix} \Big|_{\alpha_k, \beta_k, \gamma_k \approx 90^\circ}$$

$$\approx \begin{bmatrix} 1 & 0 & 0 \\ \cos \alpha_k & 1 & 0 \\ \cos \beta_k & \cos \gamma_k & 1 \end{bmatrix}. \quad (7)$$

Alignment matrix M_k is an aerospace sequence Euler angles parameterized rotation matrix, which rotates (aligns) the body reference frame b to the orthogonal sensor reference frame ko .

$$M_k = \begin{bmatrix} 1 & 0 & 0 \\ 0 & \cos \phi_k & \sin \phi_k \\ 0 & -\sin \phi_k & \cos \phi_k \end{bmatrix} \begin{bmatrix} \cos \vartheta_k & 0 & -\sin \vartheta_k \\ 0 & 1 & 0 \\ \sin \vartheta_k & 0 & \cos \vartheta_k \end{bmatrix}$$

$$\times \begin{bmatrix} \cos \psi_k & \sin \psi_k & 0 \\ -\sin \psi_k & \cos \psi_k & 0 \\ 0 & 0 & 1 \end{bmatrix} \quad (8)$$

From Eq. (6) to Eq. (8) it is evident that 12 parameters must be determined during the calibration and alignment process for each sensor triad. These parameters are divided into two groups: the group of mechanical parameters and the group of electrical parameters. Because of the diverse parameter nature, the needed frequency for the recalibration and the realignment also differs. Mechanical parameters (orthogonalization and alignment parameters) are independent of temperature and time during normal operation (which assumes no excessive shocks and stresses) and need to be determined only once during the final production phase. Electrical parameters, on the other hand, must be re-established more frequently or even at every start up (e.g. gyro bias).

When all 36 parameters for the entire MIMU are defined then the estimate \hat{u}_k for the observed physical quantity \bar{u}_k is:

$$\hat{u}_k = M_k^{-1} T_k^{-1} S_k^{-1} (\bar{y}_k - \bar{b}_k). \quad (9)$$

4.2. Accelerometer and electronic compass calibration

To minimize the design process cost, we selected such accelerometer and electronic compass calibration and alignment methods where no complex mechanical platform for the MIMU manipulation is needed. Scalar field calibration [6] and the alignment procedure presented by Včelak [7] are the appro-

priate choices in this respect. In both methods the parameters \vec{p} are established by the minimization of the objective function $O(\vec{p})$. The objective function is defined as the mean square error between the reference value u_{ref} and the corresponding data vector $u_n(\vec{p})$:

$$O(\vec{p}) = \frac{1}{N} \sum_{n=1}^N (u_{\text{ref}} - u_n(\vec{p}))^2 \quad (10)$$

where N is the number of measured values in the data vector.

The scalar field calibration method [6] is based on the fact that the magnitude of the measured gravity acceleration and Earth's magnetic field is independent of the MIMU's orientation. Consequently the gravity norm estimate ($u_n(\vec{p}) = \|\hat{a}_n\|$) by the accelerometer triad and the Earth's magnetic field norm estimate ($u_n(\vec{p}) = \|\hat{m}_n\|$) from the electronic compass are compared to the normalized local values ($u_{\text{ref}} = 1$ in both cases). The alignment parameters cannot be estimated with this method because the norm of the alignment matrix which appears in the triaxial sensor model is +1. As a consequence, the norm of the sensor triad output vector is irrespective to its alignment to the MIMU's casing. The sensitivities (s_{kx} , s_{ky} and s_{kz}), the biases (b_{kx} , b_{ky} and b_{kz}) and the orthogonalization angles (α_k , β_k and γ_k) which can be determined with the scalar field calibration are grouped in the calibration parameter vector \vec{p}_{k_cal} :

$$\vec{p}_{k_cal} = [s_{kx} \ s_{ky} \ s_{kz} \ b_{kx} \ b_{ky} \ b_{kz} \ \alpha_k \ \beta_k \ \gamma_k]^T \quad (11)$$

Since nine parameters—unknowns (s_{kx} , s_{ky} , s_{kz} , b_{kx} , b_{ky} , b_{kz} , α_k , β_k , γ_k) must be determined, at least nine equations (Eq. (6)) must be set in order to construct and solve the equation system for each sensor triad. However, in our case the equation system solving is transformed into the optimization process, therefore the construction and solving of the equations is replaced by the optimization procedure (Eq. (10)). The acquisition of the data needed for the optimization is carried out by placing the MIMU into at least nine different orientations where several data points should be acquired at each orientation. The precise knowledge of the orientation is not necessary, however it is important that the MIMU is in standstill during the data acquisition to minimize the noise in the sensor outputs. After the data set is acquired, the objective function can be minimized with one of the optimization methods. In our case the constrained Newton optimization method is used. The initial values of the parameters and the constraints are set according to the typical values quoted in the sensors' datasheets.

For the alignment procedure we have followed approach presented in [7]. With this procedure the remaining three parameters of the accelerometer and electronic compass sensor triad, i.e. the alignment Euler angles (Eq. (12)) which define the aerospace sequence parameterized rotation matrix, are obtained.

$$\vec{p}_{k_align} = [\psi_{k_align} \ \vartheta_{k_align} \ \phi_{k_align}]^T \quad (12)$$

If the aligned MIMU is rotated about the one of its sensitivity axes, then the data of the corresponding accelerometer and

electronic compass axis should be constant. But due to the sensor triad misalignment the data are deviated. The aim of the alignment procedure is to minimize this deviation. Thus the acquired data vectors ($u_n(\vec{p}) = \hat{a}_{i,n}$ for the accelerometer triad and $u_n(\vec{p}) = \hat{m}_{i,n}$ for the electronic compass) are compared to their mean values ($u_{ref} = \bar{\hat{a}}_i$ and $u_{ref} = \bar{\hat{m}}_i$, where i stands for the sensitivity axis of interest).

The alignment procedure has two steps. The first step assumes the rotation about the roll axis (x -axis) proceeding with the second rotation about the yaw axis (z -axis). In [7] the use of a non-magnetic calibration device for magnetic sensor manipulation is suggested which enables the rotations about the precisely defined orthogonal axes, however the fact that our MIMU is enclosed in an orthogonal cubic casing manufactured with a high precision CNC machine allowed us to avoid this requirement. The rotation about the desired axis is performed by putting the MIMU on the flat non-magnetic surface in the way that the axis of interest (x or z) is normal to the surface. For the best alignment results the surface should be inclined regarding to the horizontal, so that the sensitivity axis is excited also in the cross-axis direction. In the next step one revolution about the normal axis is accomplished. During the rotation the gravity acceleration and the Earth’s magnetic field are acquired in several points.

In the data processing step the deviation of x -axis data is first minimized by optimizing the heading and elevation alignment angle ($\psi_{k_align}, \vartheta_{k_align}$). With these two parameters defined, the z -axis data can be partially aligned. The complete alignment is achieved by the minimization of the partially aligned

z -axis data deviation, where the bank alignment angle (ϕ_{k_align}) is optimized.

The accelerometer triad and electronic compass calibration and alignment, according to procedure described above, were performed. Obtained parameters are presented in Fig. 6. The y -axis span of the electrical parameters’ bar charts corresponds to the parameter bounds specified in the sensors’ datasheets. From the charts it is seen that all parameters are within the bounds. The mechanical parameters are also close to the ideal values: 90° for the orthogonalization and 0° for the alignment.

4.3. Gyro calibration

The scalar field calibration is inconvenient for the gyro calibration, since the rotational platform is required. For this reason the method based on [8] is used to calibrate and align the rate gyro triad. In order to fit the complete triaxial sensor model we modified the original method in such manner that it incorporates the orthogonalization matrix as well.

According to [8] four measurements must be carried out to calibrate and align the gyro triad. The first measurement is the gyro triad bias determination. It is performed while the MIMU is kept in standstill. The bias vector \vec{b}_g is estimated as the mean value of the sensor data during the measurement period.

The other nine parameters are determined by performing the remaining three measurements. Each measurement is accomplished during the rotation about the individual sensitivity axis with known constant angular rate. The captured data are orga-

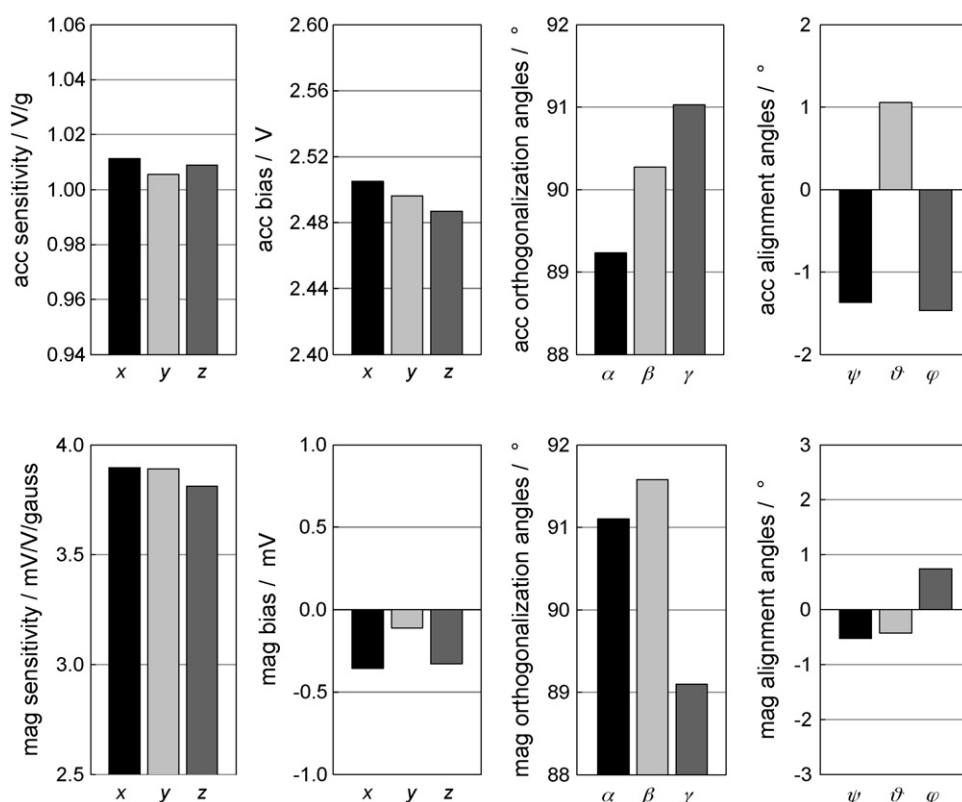


Fig. 6. Accelerometer triad and electronic compass calibration and alignment parameters (the y -axis span of the electrical parameters’ bar charts corresponds to the parameter bounds specified in the sensors’ datasheets).

nized in the matrix form. The applied angular rates are arranged on the diagonal of the matrix W_g and the bias corrected angular rate estimates (Eq. (14)) from the gyro triad are arranged in the matrix v_g , where the element $r_{g,ij}$ represents the i th gyro's output when the rotation about the j th axis is accomplished.

$$\vec{y}_g - \vec{b}_g = S_g T_g M_g \vec{u}_g \quad (13)$$

$$v_g = S_g T_g M_g W_g, \quad W_g = \begin{bmatrix} \omega_x & 0 & 0 \\ 0 & \omega_y & 0 \\ 0 & 0 & \omega_z \end{bmatrix},$$

$$v_g = \begin{bmatrix} r_{g,xx} & r_{g,xy} & r_{g,xz} \\ r_{g,yx} & r_{g,yy} & r_{g,yz} \\ r_{g,zx} & r_{g,zy} & r_{g,zz} \end{bmatrix} \quad (14)$$

Since Eq. (14) is linear (the matrices S_g , T_g and M_g are constant) the subsequent procedure can be resumed on the integrated quantities, meaning that the angular rates are substituted by the angles and no knowledge about the angular velocity is needed. However the angle of rotation needs to be known. With this assumption the angular rate matrix W_g is transformed by integration into the angle matrix A_g and the matrix v_g with bias corrected angular rate estimates is transformed into the angle estimate matrix Y_g . As a result of the integration all operations from now on are made in the angles domain (Eq. (15)).

$$Y_g = S_g T_g M_g A_g \quad (15)$$

The calibration procedure is as follows. The MIMU is placed on the flat surface and a full revolution about the surface normal axis is made. Then two successive rotations about the remaining axes are completed. The angles of rotation are written in the matrix A_g and the angle estimates in the matrix Y_g .

The matrices A_g and Y_g are composed of the measured values, while the matrices S_g , T_g , M_g are determined following the Eq. (16)–Eq. (21), where special facts about the matrices were relevant: (i) the sensitivity matrix S_g is a diagonal matrix (it can be also treated as an upper triangular matrix), (ii) the orthogonalization matrix T_g is a unit lower triangular matrix, and (iii) the alignment matrix M_g is an orthonormal matrix.

The known (measured) matrices are arranged on the left side meanwhile the unknown matrices are on the right side of Eq. (16).

$$Y_g A_g^{-1} = S_g T_g M_g \quad (16)$$

The symmetrical matrix is constructed by right multiplying each side of Eq. (16) with its transpose

$$(Y_g A_g^{-1})(Y_g A_g^{-1})^T = (S_g T_g M_g)(S_g T_g M_g)^T, \quad (17)$$

then the alignment matrix M_g is abridged, because of its orthonormality:

$$(Y_g A_g^{-1})(Y_g A_g^{-1})^T = (S_g T_g)(S_g T_g)^T. \quad (18)$$

The symmetric positive-definite matrix $(Y_g A_g^{-1})(Y_g A_g^{-1})^T$ is decomposed by the Cholesky decomposition into a lower triangular matrix $S_g T_g$ and its transpose:

$$S_g T_g = \text{chol}[(Y_g A_g^{-1})(Y_g A_g^{-1})^T]^T. \quad (19)$$

The sensitivity and the orthogonalization matrices are retrieved by the LU decomposition of the matrix $S_g T_g$, where the orthogonalization matrix T_g is a lower and the sensitivity matrix S_g an upper triangular matrix:

$$[T_g, S_g] = \text{LU}(S_g T_g). \quad (20)$$

Finally the alignment matrix M_g is obtained by the following manipulation of matrices:

$$M_g = T_g^{-1} S_g^{-1} Y_g A_g^{-1}. \quad (21)$$

The gyro triad calibration and alignment was performed as well. Acquired parameters are exposed in Fig. 7. The parameters of the gyro triad are within the specified bounds, similar as in the accelerometer triad and electronic compass case.

5. Data fusion algorithm

Due to the unbounded gyro rate integration error, the gyro-derived orientation must be augmented with the accelerometer and electronic compass data to assure long-term stability and orientation information reliability. The accelerometer triad and

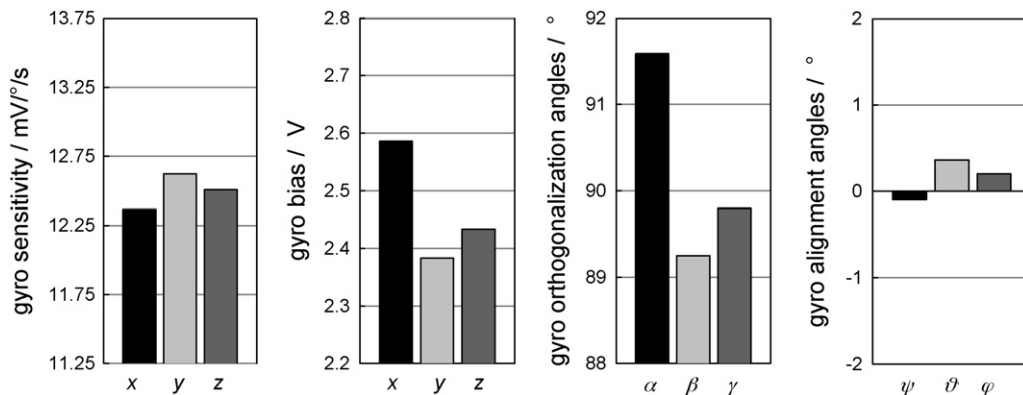


Fig. 7. Gyro triad calibration and alignment parameters (the y-axis span of the electrical parameters' bar charts corresponds to the parameter bounds specified in the sensors' datasheets).

the electronic compass act as an aiding system (AS) for the gyroscopes. For the fusion of the different sensor data an adaptive Kalman filter concept is proposed and implemented.

A MIMU model in the state space is derived. The three Euler angles (ψ -heading, ϑ -elevation and ϕ -bank) present the system state vector \tilde{x} . The gyro rate integration is represented by the Eq. (22) and the system state measurements \tilde{z} , taken by the accelerometer triad and electronic compass, by Eq. (23).

$$\tilde{x}_k = \Phi_{k-1}\tilde{x}_{k-1} + B_{k-1}\tilde{u}_{k-1} + \tilde{w}_{k-1}; \quad (22)$$

$$\tilde{x}_k = \begin{bmatrix} \psi_k \\ \vartheta_k \\ \phi_k \end{bmatrix} \text{state vector, } \tilde{u}_k = \begin{bmatrix} \omega_{x,k} \\ \omega_{y,k} \\ \omega_{z,k} \end{bmatrix} \text{input vector,}$$

$\Phi_k = I_3$ state transition matrix,

$$B_k = \begin{bmatrix} 0 & \sin \phi_k \sec \vartheta_k & \cos \phi_k \sec \vartheta_k \\ 0 & \cos \phi_k & -\sin \phi_k \\ 1 & \sin \phi_k \tan \vartheta_k & \cos \phi_k \tan \vartheta_k \end{bmatrix}$$

input coupling matrix

$$\tilde{z}_k = H_k\tilde{x}_k + \tilde{v}_k, \quad (23)$$

$H_k = I_3$ measurement sensitivity matrix

Two noise sources with belonging covariance matrices are also included in the model: the process noise vector \tilde{w}_k with the covariance matrix Q_k and the measurement noise vector \tilde{v}_k with the covariance matrix R_k .

Kalman filter data fusion process is divided into two steps: a time update and a measurement update. Time update is executed at a fixed rate and propagates the system state \tilde{x}_k (Eq. (24)) and the error covariance matrix P_k (Eq. (25)) further in time. Predicted (*a priori*) values ($\hat{\tilde{x}}_k^-$ and P_k^-) are then passed to the measurement update which occurs whenever the orientation information from the aiding system is available. During the measurement update the Kalman gain K_k is calculated in the first place (Eq. (26)). Then the state vector estimate (Eq. (27)) and the error covariance (Eq. (28)) correction based on the state measurement, is carried out. After that, the corrected (*a posteriori*) values ($\hat{\tilde{x}}_k$ and P_k) are obtained and the full cycle is accomplished [11].

Discrete Kalman filter time update equations—*prediction*:

$$\hat{\tilde{x}}_k^- = \Phi_{k-1} + B_{k-1}\tilde{u}_{k-1} \quad (24)$$

$$P_k^- = \Phi_{k-1}P_{k-1}\Phi_{k-1}^T + Q_{k-1} \quad (25)$$

$\hat{\tilde{x}}_k^-$ —predicted (*a priori*) value of the estimated state vector, P_k^- —predicted (*a priori*) error covariance matrix and Q_k —process noise covariance matrix.

Discrete Kalman filter measurement update equations—*correction*:

$$K_k = P_k^- H_k^T (H_k P_k^- H_k^T + R_k)^{-1} \quad (26)$$

$$\hat{\tilde{x}}_k = \hat{\tilde{x}}_k^- + K_k(z_k - H_k\hat{\tilde{x}}_k^-) \quad (27)$$

$$P_k = (I - K_k H_k) P_k^- \quad (28)$$

K_k —Kalman gain, R_k —measurement noise covariance matrix, $\hat{\tilde{x}}_k$ —corrected (*a posteriori*) value of the estimated state vector, P_k —corrected (*a posteriori*) error covariance matrix.

Since the system dynamics is varying, the noise covariance matrix of the process Q_k (Eq. (29)) and of the measurement R_k (Eq. (30)) are adaptively modified during the runtime to maximally suit the variable characteristics of the process and measurement noise.

$$Q_k = \begin{bmatrix} \sigma_{Q,k}^2 & 0 & 0 \\ 0 & \sigma_{Q,k}^2 & 0 \\ 0 & 0 & \sigma_{Q,k}^2 \end{bmatrix} \quad (29)$$

$$R_k = \begin{bmatrix} \sigma_{\psi,k}^2 & 0 & 0 \\ 0 & \sigma_{\vartheta,k}^2 & 0 \\ 0 & 0 & \sigma_{\phi,k}^2 \end{bmatrix} \quad (30)$$

The process noise is increasing with the magnitude of the rotational motion (Eq. (31)) due to the limited bandwidth of the sensors; so the process covariance is linearly increased (Eq. (32)) during the intensified dynamic rotational manoeuvres, as more noise is injected in the process.

$$\Omega_k = \sqrt{\omega_{x,k}^2 + \omega_{y,k}^2 + \omega_{z,k}^2} \quad (31)$$

$$\sigma_{Q,k}^2 = \frac{\sigma_{Q_{hi}}^2 - \sigma_{Q_{lo}}^2}{\Omega_{\max}} \Omega_k + \sigma_{Q_{lo}}^2; \quad (32)$$

$$\begin{aligned} \Omega_{\max} &= \sqrt{\omega_{x,\max}^2 + \omega_{y,\max}^2 + \omega_{z,\max}^2} \\ &= \sqrt{(150^\circ/s)^2 + (150^\circ/s)^2 + (150^\circ/s)^2}, \end{aligned}$$

$$\Omega_{\max} = 260^\circ/s, \quad \sigma_{Q_{lo}}^2 = 0.01, \quad \sigma_{Q_{hi}}^2 = 0.05$$

The measurement noise and consecutively the measurement noise covariance matrix (Eq. (30)) depend on the conditions in which the system state measurements were taken. The term $\sigma_{\psi,k}^2$ is coupled with the electronic compass, the magnetic aiding system (MAS) uncertainty, meanwhile the terms $\sigma_{\vartheta,k}^2$ and $\sigma_{\phi,k}^2$ are linked with the accelerometer, the inertial aiding system (IAS), uncertainty. First of all we must assure that the Euler angles (system state) measurements from the IAS and MAS are correct. In the case of IAS a static activity detection algorithm is implemented, while the norm of the magnetic field and the dip angle are observed for the MAS.

If the gravity is the only force affecting the MIMU then the acceleration vector is moving on the sphere with the radius of 1 g. This condition must hold for certain amount of time before the IAS measurement is stated valid, to avoid false triggers which may occur when the dynamic acceleration adds together with the gravity in such way that their resultant lies on the sphere or the vector trajectory passes through it [12].

The MAS validity is based on the deviation of the magnetic field norm and the dip angle. If the magnetic vector lies on the

sphere with the normalized radius of 1 and the magnetic field inclination is correct then the MAS measurement is stated as valid.

After the AS measurements are established to be valid, the measurement covariance matrix (Eq. (30)) is determined. The variance terms are dependent of the magnitude deviation from the unity value (the AS trust interval is the maximum allowed deviation from the unity). If the magnitude is close to the unity then the measurement uncertainty is low, but when the magnitude moves off, the uncertainty is linearly increased as the noise and additional disturbances affect the measurements taken by the AS:

$$\sigma_{R,k}^2 = \begin{cases} \frac{\sigma_{Rhi}^2 - \sigma_{Rlo}^2}{\text{AS trust interval}} (\|k\| - 1) + \sigma_{Rlo}^2, & \|k\| > 1 \\ -\frac{\sigma_{Rhi}^2 - \sigma_{Rlo}^2}{\text{AS trust interval}} (\|k\| - 1) + \sigma_{Rlo}^2, & \|k\| < 1 \end{cases},$$

$$\|k\| = \text{acceleration or magnetic field norm}, \quad \sigma_{Rlo}^2 = 10,$$

$$\sigma_{Rhi}^2 = 100, \quad \text{AS trust interval} = 0.01. \quad (33)$$

6. Experimental results

For the evaluation of the calibration, alignment and implemented data fusion algorithm, several dynamic motion sequences were monitored with the MIMU. The calculated attitude and heading angles were compared to the reference measurement done by the optical kinematic measurement system Optotrak 3010 by the Northern Digital, Inc. (Fig. 8), which measures the position of infrared markers (IR LEDs) in space with accuracy up to 0.3 mm and sampling frequency up to 2000 Hz. The sensor data were sampled with the sampling frequency of 100 Hz and stored on the PC. Post-processing according to the previously described algorithm was executed to determine the attitude and heading trend during the test sequences.

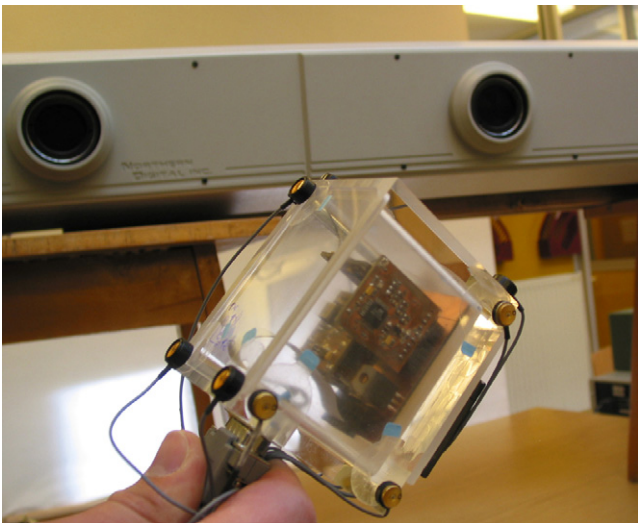


Fig. 8. Measurement setup.

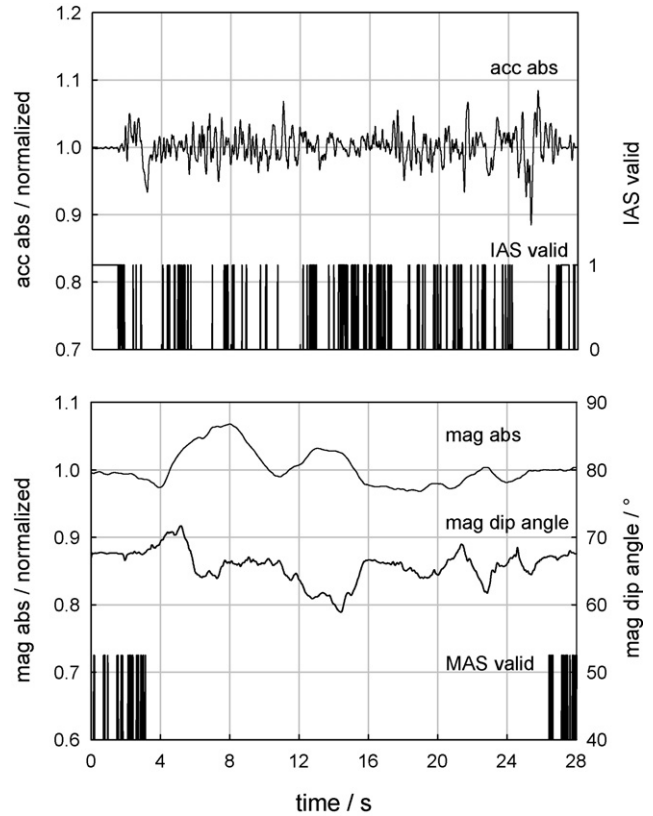


Fig. 9. IAS and MAS test sequence parameters.

The MIMU performance results are demonstrated on a highly dynamic motion sequence ($\Omega_{\max} = 150^\circ/\text{s}$, $\|a\|_{\max} = 1.1 \text{ g}$), which covered entire operating range (Fig. 10), where only the gimbal lock regions were avoided (approx. $|\vartheta| > 80^\circ$). The motion sequence was performed in a partially distorted Earth's magnetic field. The maximum norm of the magnetic field was approx. 7% larger than the normal value, which is more than enough to compromise the MAS heading measurement. The IAS and MAS parameter course are presented in Fig. 9. The time slots where the AS data are taken into the consideration are clearly indicated by the signals IAS valid and MAS valid. The norms of the acceleration and the magnetic field, as well as the magnetic field dip angle are also presented in Fig. 9.

The data fusion algorithm despite its simplicity managed to estimate the orientation successfully as the root mean square (rms) Euler angle errors remained within the limits of 1.2° : heading error, 1.13° rms; elevation error, 0.77° rms; bank error, 1.05° rms (Fig. 10). Under the intensive dynamic manoeuvres the momentary orientation error increased for a short time to maximally 3.4° (heading error: 3.38° max, elevation error: 2.33° max, bank error: 3.19° max), but when the dynamics settled down the orientation error decreased and the orientation accuracy improved. If only the gyroscopes would be used to monitor the orientation then the orientation error would increase with time and the orientation information would be totally incorrect after a short period of time. In our test case the gyro accumulating error increased to 2.75° after 28 s of motion, and the momentary errors were as high as 6.6° (Fig. 10).

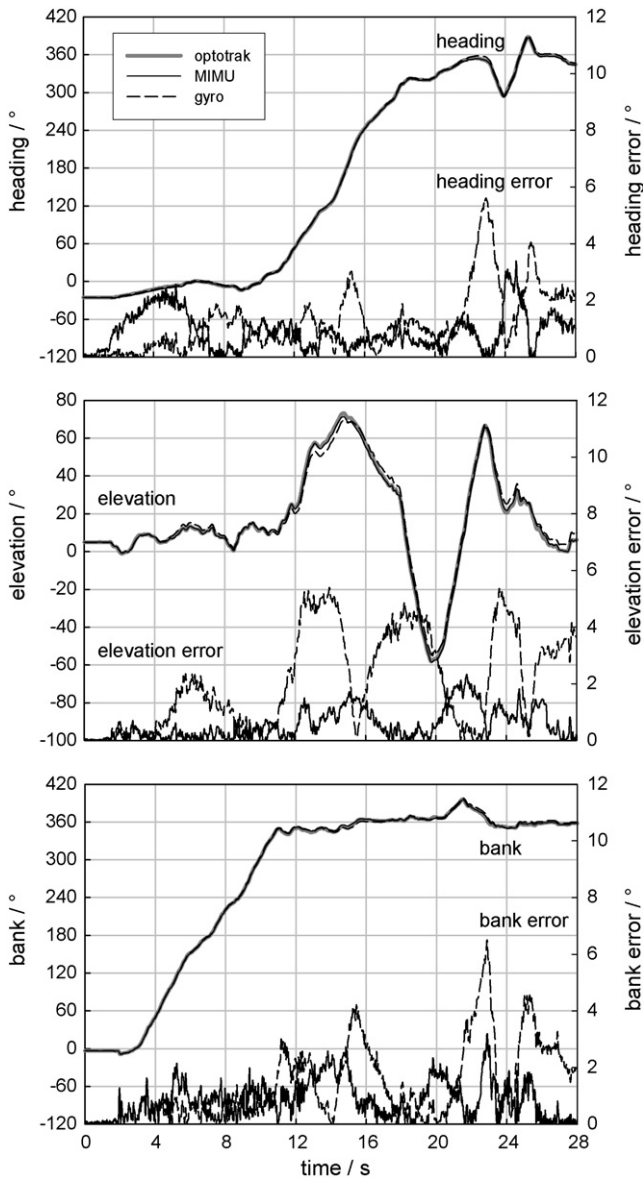


Fig. 10. Test sequence data.

Adaptive varying of the process and measurement covariance matrices demonstrated as a good choice since a trade-off between the noise rejection and drift cancellation could not be managed so successfully in the case of the invariable process and measurement covariance matrices, as at high gains the drift effect is suppressed but a lot of AS noise is coupled into the orientation data. On the contrary, if the gain is constantly low then the noise is not so visible but the orientation information could still be drifting due to insufficient AS's data weighting.

7. Conclusion

A small modular inertial measurement unit was designed and realized. For motion sensing we used the low-cost MEMS inertial sensors and AMR sensors for magnetic field sensing. Such choice of sensors resulted in very reliable and affordable IMU.

The MIMU was calibrated and aligned with the developed simple but very effective procedures which do not need any complex mechanical platforms for MIMU manipulation. An innovative adaptive Kalman filter data fusion concept for attitude and heading determination was introduced, implemented and evaluated. The algorithm showed remarkable performance in the orientation determination as the average rms error was less than 1.2° over the entire applicable operating range.

Since the MIMU is designed in a modular way some additional types of sensor units can be easily added. For example, if the MIMU is used as an AHRS for an UAV, a pressure sensor unit for altitude and speed measurement or a GPS receiver as an absolute position definition system or even as an aiding system for the gyro data augmentation can be attached to the control unit thus a complete control system for UAV guidance and control is obtained.

Acknowledgement

The authors wish to thank Damir Franetič for helpful discussions.

References

- [1] S.K. Hong, Fuzzy logic based closed-loop strapdown attitude system for unmanned aerial vehicle (UAV), *Sens. Actuator A* 107 (2003) 109–118.
- [2] D. Loebis, R. Sutton, J. Chundley, W. Naeem, Adaptive tuning of a Kalman filter via fuzzy logic for an intelligent AUV navigation system, *Control Eng. Pract.* 12 (2004) 1531–1539.
- [3] H.J. Luinge, P.H. Veltink, Inclination measurement of human movement using a 3-D accelerometer with autocalibration, *IEEE Trans. Neural. Syst. Rehabil. Eng.* 12 (2004) 112–121.
- [4] Analog devices ADXRS150 datasheet, www.analog.com.
- [5] Honeywell HMC1001/1002 datasheet, www.magneticsensors.com.
- [6] I. Skog, P. Händel, Calibration of a Mems Inertial Measurement Unit, XVIII IMEKO World Congress, Metrology for a Sustainable Development, Rio de Janeiro, Brazil, 2006, pp. 17–22.
- [7] J. Včelak, P. Ripka, J. Kubik, A. Platil, P. Kašpar, AMR navigation systems and methods of their calibrations, *Sens. Actuator A* 123–124 (2005) 122–128.
- [8] F. Ferraris, U. Grimaldi, M. Parvis, Procedure for effortless in-field calibration of three-axis rate gyros and accelerometers, *Sens. Mater.* 7 (1995) 311–330.
- [9] J.B. Kuipers, *Quaternions and Rotation Sequences*, Princeton University Press, Princeton, NJ, 1999, pp. 84–86.
- [10] B.B. Pant, M. Caruso, Magnetic sensor cross-axis effect, AN-205, Honeywell, 1996.
- [11] G. Welch, G. Bishop, *An Introduction to the Kalman Filter*, University of North Carolina, Chapel Hill, 2004, pp. 4–6.
- [12] H. Rehbinder, X. Hu, Drift-free attitude estimation for accelerated rigid bodies, *Automatica* 40 (2004) 653–659.

Biographies

David Jurman received the university diploma degree in electrical engineering at University of Ljubljana, Slovenia in 2004. From 2004 he is employed at the same faculty as a junior researcher and is working on inertial sensors and embedded systems as a PhD student.

Marko Jankovec received the PhD degree in electrical engineering at University of Ljubljana, Slovenia, in 2004. From 2001 he is a teaching assistant at the same faculty. His research includes thin-film optoelectronic devices and materials, electronic noise in detectors and electronic circuits.

Roman Kamnik received the PhD degree in electrical engineering at University of Ljubljana, Slovenia, in 1999. Currently he is an assistant professor at the Faculty of Electrical Engineering, University of Ljubljana. His research interests are focused to analysis and synthesis of multibody systems motion with the applications to biomedical engineering, robotics and transport.

Marko Topič received the PhD degree in electrical engineering at University of Ljubljana, Slovenia, in 1996. Currently he is a full professor at the Faculty of Electrical Engineering, University of Ljubljana, where he is a head of the Laboratory of Photovoltaics and Optoelectronics. His research interests include semiconductor materials, electron devices, optoelectronics, electronic circuits, and reliability engineering.